Geophysical Journal International

Geophys. J. Int. (2011) **187,** 690–704 doi: 10.1111/j.1365-246X.2011.05187.x

The evolution of a magnetic field subject to Taylor's constraint using a projection operator

Philip W. Livermore,[1,2]* Glenn Ierley[1] and Andrew Jackson[2]

[1]*Institute of Geophysics and Planetary Physics, Scripps Institution of Oceanography, UCSD, San Diego, USA. E-mail p.w.livermore@leeds.ac.uk*
[2]*Institut für Geophysik, ETH, Zürich, Switzerland*

Accepted 2011 August 8. Received 2011 July 25; in original form 2010 March 23

SUMMARY

In the rapidly rotating, low-viscosity limit of the magnetohydrodynamic equations as relevant to the conditions in planetary cores, any generated magnetic field likely evolves while simultaneously satisfying a particular continuous family of invariants, termed Taylor's constraint. It is known that, analytically, any magnetic field will evolve subject to these constraints through the action of a time-dependent coaxially cylindrical geostrophic flow. However, severe numerical problems limit the accuracy of this procedure, leading to rapid violation of the constraints. By judicious choice of a certain truncated Galerkin representation of the magnetic field, Taylor's constraint reduces to a finite set of conditions of size $O(N)$, significantly less than the $O(N^3)$ degrees of freedom, where N denotes the spectral truncation in both solid angle and radius. Each constraint is homogeneous and quadratic in the magnetic field and, taken together, the constraints define the finite-dimensional *Taylor manifold* whose tangent plane can be evaluated. The key result of this paper is a description of a stable numerical method in which the evolution of a magnetic field in a spherical geometry is constrained to the manifold by projecting its rate of change onto the local tangent hyperplane. The tangent plane is evaluated by contracting the vector of spectral coefficients with the *Taylor tensor*, a large but very sparse 3-D array that we define. We demonstrate by example the numerical difficulties in finding the geostrophic flow numerically and how the projection method can correct for inaccuracies. Further, we show that, in a simplified system using projection, the normalized measure of Taylorization, τ, may be maintained smaller than $O(10^{-10})$ (where $\tau = 0$ is an exact Taylor state) over 1/10 of a dipole decay time, eight orders of magnitude smaller than analogous measures applied to recent low Ekman-number geodynamo models.

Key words: Numerical approximations and analysis; Electromagnetic theory; Dynamo: theories and simulations; Planetary interiors.

1 INTRODUCTION

1.1 Geophysical motivation

Many physical systems evolve subject to known invariants, of which perhaps the best known are energy, momentum and mass; such quantities are conserved along any trajectory of the system. In many cases, these constraints derive directly from the governing equations and, if analytic solutions were available, they would be automatically satisfied. In other systems the constraints stem from considerations of internal structure where, for instance, a collection of point masses representing the vertices of a robot arm are connected together by invariant lengths of material. In all cases, barring specific design considerations, any output of a numerical scheme used for evolving such a system is likely not to satisfy the constraints due, at the very least, to the accumulation of numerical errors. In many applications, obeying the constraints is not just an academic exercise but is crucial for understanding the model and suppressing numerical instabilities. Applications for constrained dynamics span a wide range of topics that include fluid dynamics (Salmon 2005), robotics (Hong *et al.* 2005), interaction of complex solid bodies (e.g. computer gaming, Fox *et al.* 2000) and molecular dynamics (Frenkel & Smit 2002).

Our interest in constrained dynamics is motivated by something quite different: the mechanism that effects the generation and sustenance of magnetic fields in the liquid outer core of the Earth. The so-called geodynamo is ultimately powered by the secular cooling of the planet, actuating rotationally influenced buoyancy-driven convection. This motion drives a self-excited dynamo process, sustaining the field against decay. A full understanding of this magnetohydrodynamic system requires knowledge of the spatial structure and evolution of the flow **u** and magnetic field **B**, described by the

*Now at: School of Earth and Environment, University of Leeds, Leeds, UK LS2 9JT.

non-dimensionalized Navier–Stokes and induction equation

$$\hat{\mathbf{z}} \times \mathbf{u} = -\nabla p + \tilde{R}_a \, T(\mathbf{r}) \hat{\mathbf{r}} + [\nabla \times \mathbf{B}] \times \mathbf{B} + \left[- R_o \left(\frac{\partial \mathbf{u}}{\partial t} + (\mathbf{u} \cdot \nabla)\mathbf{u} \right) + E \, \nabla^2 \mathbf{u} \right], \tag{1}$$

$$\frac{\partial \mathbf{B}}{\partial t} = \nabla \times (\mathbf{u} \times \mathbf{B}) + \nabla^2 \mathbf{B}, \qquad \nabla \cdot \mathbf{B} = \mathbf{0} \tag{2}$$

along with an equation for the temperature anomaly T, supplying buoyancy, which is not needed in our discussion. The buoyancy force points in the radial direction, defined by the unit vector $\hat{\mathbf{r}}$; $\hat{\mathbf{z}}$ is a unit vector along the rotation axis and p denotes the pressure. Following Fearn (1998), the equations have been non-dimensionalized based on typical length and timescales of the radius of the outer core and the *a priori* magnetic diffusion time of around 10^5 years. Typical conditions imposed on the outer boundary are those of an impenetrable, non-slip and electrically insulating exterior. If included in the geometry, an inner core is usually modelled as electrically conducting with a non-slip and impenetrable surface. The remaining parameters are the Rossby number, R_o (measuring inertia), the Ekman number, E (measuring viscosity) and a (modified) Rayleigh number $\tilde{R}_a$ (measuring the buoyancy force). The parameters R_o and E are both small, taking typical values of $O(10^{-9})$ and $O(10^{-15})$, respectively, in the Earth's core. Therefore, to a good approximation, it is believed that the rightmost parenthesized terms of (1) may be neglected, resulting in the 'magnetostrophic balance' between the Coriolis force, pressure, buoyancy and the Lorentz force. The magnetostrophic system is of considerable interest as it describes the slow evolution of the geomagnetic field (on millenial timescales), perhaps being able to explain the longstanding dominance of the axially symmetric dipolar component of the field, along with dynamics such as geomagnetic reversals. Furthermore, superimposed on this background state are faster dynamics such as torsional waves or oscillations, for which there is mounting observational evidence (Jault *et al.* 1988; Gillet *et al.* 2010).

Turning back to the detail of the magnetostrophic approximation: discarding the two non-dimensionally small terms in (1) results in two significant algebraic changes to the equations. First, the elimination of viscosity reduces the order of the highest derivative occurring, and thus also the number of boundary conditions we can impose. Modelling the boundaries as impenetrable provides the required number of conditions: we need not (and cannot) impose that the boundaries are non-slip (as we might if viscosity was retained). This procedure is equivalent to solving for the free-stream component of flow in a viscous calculation (Taylor 1963). Second, neglecting inertia renders (1) a diagnostic equation for $\mathbf{u}$ rather than prognostic, and $\mathbf{u}$ is implicitly determined through knowledge of $\mathbf{B}$ and T. Note that the system, as a whole, remains dissipative even with zero viscosity due to the existence of magnetic diffusion, describing the energy lost into Ohmic heating. Despite huge advances in parallel computing in the last few decades, the low-viscosity low-inertia regime of (1) remains out of reach due to the existence of very short time and small spatial scales which present a significant numerical obstacle (Kono & Roberts 2002). The limiting case of $R_o = E = 0$ has been largely inaccessible due to a particular theoretical hurdle known as Taylor's constraint, an accurate and efficient numerical treatment of which is the focus of this paper.

Some 48 yr ago, Taylor (1963) proved a necessary condition of any solution to the magnetostrophic equations, now termed Taylor's constraint. By considering an average over geostrophic contours [cylinders of fluid $C(s)$, coaxial with the rotation axis], he showed

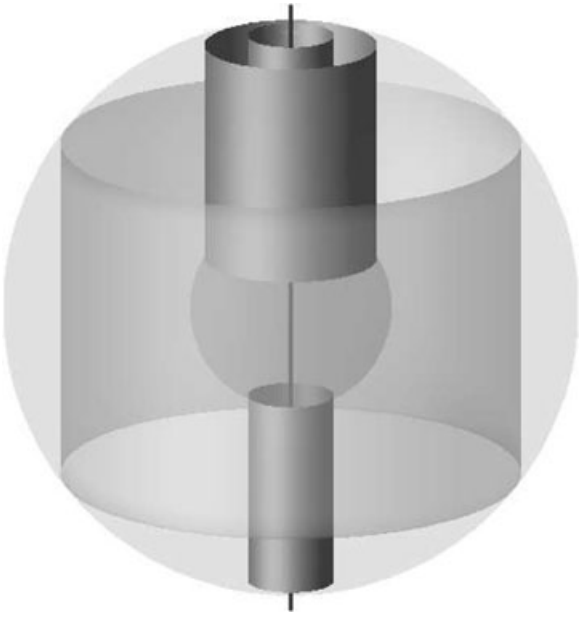

Figure 1. Example cylinders over which Taylor's constraint is defined, each of which is coaxial with the rotation axis and touches the edge of the core at its extremities. In a full sphere, there is just one family of cylinders. In a spherical shell, there are three: outside the tangent cylinder, and above and below the inner core.

that

$$\mathcal{T}(s) \equiv \int_{C(s)} \left([\nabla \times \mathbf{B}] \times \mathbf{B} \right)_\phi \, s \, \mathrm{d}\phi \, \mathrm{d}z = 0, \tag{3}$$

where (s, ϕ, z) are cylindrical coordinates and $(\,)_\phi$ signifies the azimuthal component. This condition follows because the Coriolis, pressure and buoyancy forces vanish under this average and so, therefore, the Lorentz force must also. Under the assumption that the core is a full sphere (with no inner core), (3) describes a single infinite member family of constraints parametrized by the cylindrical radius $0 \leq s \leq 1$. In a more realistic (although more complex) geometry of a spherical shell, there are three families of geostrophic contours $C(s)$, those outside the so-called tangent cylinder (the cylinder aligned with the rotation axis and tangent to the inner core at the equator) and those inside the tangent cylinder above and below the inner core. Examples of such cylinders are shown in Fig. 1.

Taylor's constraint presents a formidable obstacle. Not only does it involve cylindrical averages, rather awkward when quantities are naturally expressed in spherical polar coordinates, but, ostensibly, it supplies infinitely many independent conditions (one for each possible choice of cylinder). However, in a fully spectral method with a finite number of degrees of freedom, the Taylor integral, $\mathcal{T}(s)$ (in 3), is a finite algebraic object and can be rendered zero by applying a finite number of constraints to $\mathbf{B}$ (Livermore *et al.* 2008). Furthermore, by judicious choice of method, the number of constraints can be made significantly fewer than the number of degrees of freedom and solutions, known as Taylor states, exist (see Section 2.1 for more detail). In a typical model of moderate resolution, the number of constraints, each quadratic in $\mathbf{B}$, may number $O(10)$–$O(100)$, which must simultaneously be satisfied in any solution of (1) and (2) with $E = R_o = 0$. Within the finite multidimensional space of magnetic field spectral coefficients that satisfy the conditions

appropriate for an electrically insulating exterior, Taylor's constraint defines a multidimensional surface which we term the *Taylor manifold*, defined by the intersection of quadratic surfaces associated with each individual constraint. Any solution to the inertia-free inviscid geodynamo equations must necessarily evolve along this manifold, just as a Hamiltonian system evolves along a surface of constant energy. The purpose of this paper is to present an initial study of how this can be achieved numerically.

1.2 Taylor's time-evolution algorithm

In many fluid dynamical systems the inertial terms are important and hence the Navier–Stokes equations are prognostic. However, here smallness of Rossby number means that inertial terms are dropped for the magnetostrophic system and so the equations for velocity are diagnostic, determined according to Taylor's prescription (3) for a unique flow. The evolution of the flow is slaved to that of magnetic and temperature fields and hence of comparable smoothness in time.

Taylor showed that the flow can be written as two components

$$\mathbf{u} = \mathbf{u}_{\rm mag} + u_g(s)\,\hat{\phi}, \tag{4}$$

comprising what we denote here as the magnetostrophic flow and the geostrophic flow. Only the magnetostrophic flow, quadratic in $\mathbf{B}$, may be determined from (1) (using, for instance, the integral approach of Taylor), since $u_g(s)$, the geostrophic component of flow, represents a null space of solution. This can be easily seen by noting that $\hat{\mathbf{z}} \times u_g(s)\hat{\phi} = -u_g(s)\hat{\mathbf{s}}$, which can be absorbed into the pressure gradient. The undetermined geostrophic component of flow is fixed by imposing the additional dynamical statement that the time-derivative of Taylor's constraint must also be zero. Taylor showed that u_g satisfies a linear second-order ordinary differential equation whose coefficients are non-linear in the magnetic field:

$$\alpha(s)\frac{\mathrm{d}^2}{\mathrm{d}s^2}\left(\frac{u_g(s)}{s}\right) + \beta(s)\frac{\mathrm{d}}{\mathrm{d}s}\left(\frac{u_g(s)}{s}\right) = G(s), \tag{5}$$

where

$$\alpha(s) = \int_{C(s)} s\,B_s^2\,s\,\mathrm{d}\phi\,\mathrm{d}z,$$

$$\beta(s) = \int_{C(s)} \left[2B_s^2 + s\,\mathbf{B}\cdot\nabla B_s\right] s\,\mathrm{d}\phi\,\mathrm{d}z, \tag{6}$$

and $G(s)$ is a complex expression depending on $\mathbf{u}_{\rm mag}$ and $\mathbf{B}$; $C(s)$ is any geostrophic cylinder.[1] Although α and β are both quadratic in $\mathbf{B}$, $G(s)$ is quartic in $\mathbf{B}$ and thus u_g is quadratic in $\mathbf{B}$ as is $\mathbf{u}_{\rm mag}$.

The equation for u_g is an *exact* statement and, although somewhat involved, this method presents a possible quasi-analytic scheme by which the magnetostrophic equations can be solved. In essence the algorithm is

loop

1. $\mathbf{u}_{\rm mag}(t_n) = g(\mathbf{B}(t_n), T(t_n))$
2. Find $u_g(t_n) = u_g(\mathbf{u}_{\rm mag}(t_n), \mathbf{B}(t_n))$
3. $\mathbf{u}(t_n) = \mathbf{u}_{\rm mag}(t_n) + u_g(t_n)\,\hat{\phi}$
4. $\mathbf{B}(t_{n+1}) = f(\mathbf{u}(t_n), \mathbf{B}(t_n))$
5. $T(t_{n+1}) = h(\mathbf{u}(t_n), T(t_n))$

end loop

where f and h represent time-evolution schemes applied to (2) and for the temperature T; g is the method of computing $\mathbf{u}_{\rm mag}(\mathbf{B}, T)$ and t_n is discrete time. Note that $\mathbf{u}(t_n)$ depends only on previous states of the flow through dependence on $\mathbf{B}$ and T.

This algorithm, although rather elegant, has some fairly serious difficulties when implemented numerically, as illustrated by previous attempts (e.g. Fearn & Proctor 1987). The first problem is to find an exact Taylor state that we may use as an initial condition. Although some isolated examples exist in the literature (e.g. Hollerbach & Ierley 1991), a generalized approach has only recently come to light (Livermore *et al.* 2009, 2010). The second problem is how to keep the magnetic field on the Taylor manifold. In Taylor's method, if the initial state is on the manifold and the time derivative of Taylor's constraint remains identically zero (through the action of the geostrophic flow so defined) then Taylor's constraint will be satisfied for all time. This quasi-analytic algorithm contains the implicit assumption that $u_g(s)$, the geostrophic flow, is handled analytically. However, in any practical scheme, since the coefficients of the required ordinary differential equation depend in a complicated way on s, this is not usually possible and so one would need to find u_g numerically. Two associated computational problems, described later, both result in inaccurate treatment of u_g which will not confine the trajectory of the magnetic field to the Taylor manifold for more than a short interval; thus major problems hamper a direct application of Taylor's method.

The first issue is that we might adopt a truncated spectral expansion to find u_g, anticipating that u_g is smooth and its spectral representation should converge exponentially fast. However, this is not so: although u_g may be smooth, typical expansions converge slowly (see the example in Section 3.2). The coefficients of the ODE are numerically costly cylindrical averages of rather complex functions: α and β are quadratic in $\mathbf{B}$, and G is quartic in $\mathbf{B}$ through its dependence on $\mathbf{u}_{\rm mag}$. The high computation cost that arises is due, not only to the fact that $\mathbf{B}$ is represented in spherical coordinates that are not easily averaged in cylindrical coordinates, but because $\mathbf{B}$ may be small scale necessitating a large number of quadrature points. Furthermore, α, β and G must be recomputed at each time step, since $\mathbf{B}$ itself changes in time. It is therefore apparent that, due to computational limitations, it may not practical to compute u_g to anything more than a moderate resolution which, depending on the rate of convergence, may mean that u_g is significantly underresolved.

The second issue is, quite independent of the above, the discretization error in the representation of $\frac{\partial \mathbf{B}}{\partial t}$. Even if u_g is known to high precision, the estimate of $\frac{\partial \mathbf{B}}{\partial t}$ must be projected onto the numerical discretization used to represent the magnetic field, commonly a truncated fully spectral approach. Thus after projection onto the discretization, information may be lost and $\frac{\partial \mathbf{B}}{\partial t}$ may no longer lie in the tangent plane of the manifold.

Both of the above effects will be present in any discretized scheme and, as shown by an example in Section 3.2, will lead to a rapid divergence from the Taylor manifold. Of course, the rate of divergence will reduce with increasing truncation in both space and time, as the numerical scheme will be able to represent to a much higher accuracy the required dynamics. In this paper we discuss a modification to the algorithm that confines the magnetic field to the Taylor manifold, even if u_g is not handled with high precision.

1.3 Overview of the projection method

The key problem with Taylor's method, as will be demonstrated by an example in Section 3.2, is that errors in representing either u_g or its action on the magnetic field may send the trajectory of $\mathbf{B}$

[1] Note the typographic error in Taylor's paper in the coefficient β (as can be confirmed by dimensional analysis).

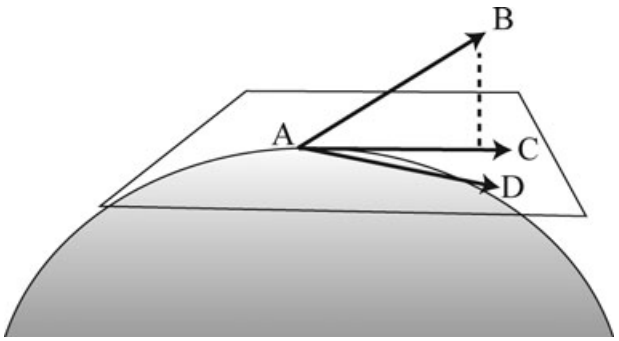

Figure 2. Consider a point A on the Taylor manifold (depicted, with artistic license, as the surface of the solid ellipse) with local tangent plane as shown. The instantaneous exact vector $\frac{\partial \mathbf{B}}{\partial t}$, computed with an analytic u_g, points in the direction AD (in plane); $\frac{\partial \mathbf{B}}{\partial t}$ computed using an inexact u_g points in the direction AB (out of plane). The evolution may be corrected by projecting AB onto AC, onto the tangent-plane of the manifold; although both AC and AD lie in the tangent plane, their in-plane components differ.

rapidly off the manifold; that is, $\frac{\partial \mathbf{B}}{\partial t}$ from (2) will quickly diverge from the local tangent hyperplane. Without correction, Taylor's constraint would be violated after a potentially small number of time steps. As we will explain in more detail in Section 2.2, it is always possible to construct the local tangent hyperplane at any point on the Taylor manifold. Given any Taylor state $\mathbf{B}$, we define $\mathcal{P}_{\mathbf{B}}$ to be the projection onto the local tangent plane. One way of avoiding numerical problems is to evolve the magnetic field using the refined estimate of its rate of change: $\mathcal{P}_{\mathbf{B}}(\frac{\partial \mathbf{B}}{\partial t})$.

The key ideas are illustrated in Fig. 2. Suppose that the system lies at point A on the Taylor manifold (depicted by the surface of the solid ellipse). If we compute $\frac{\partial \mathbf{B}}{\partial t}$ (from 2 and 4) using an inaccurate representation of u_g it will, in general, point off the manifold in the direction AB; an exact treatment of u_g would ensure that $\frac{\partial \mathbf{B}}{\partial t}$ lies in the local tangent plane in the direction AD. Numerically, we may correct the trajectory AB to AC by projecting it down onto the local tangent plane, discarding the out-of-plane component. How this may be achieved computationally is the focus of the remainder of the paper.

1.4 Recent work on constrained systems

Having introduced the problem under consideration, it is of interest to review briefly other constrained dynamical models in the current literature, which may be broadly divided into two classes. First, there are hydrodynamical models principally involving the Navier–Stokes and continuity equations, describing conservation of momentum and mass. Depending on the assumptions made, further constraints may be derived directly, for example: energy, potential vorticity (Müller 1995) and flow helicity (Moffatt 1969). Importantly, the constraints are so few in number that it is possible to construct numerical schemes in which they are satisfied exactly (e.g. Marsden *et al.* 1998; Salmon 2005). One the one hand, the equations that we consider in this paper are an extension of hydrodynamics, that is, we allow the fluid to be electrically conducting and consider the additional complication of a magnetic field. However, the number of constraints that enter our problem is considerably more than those relating to hydrodynamic studies [typically $O(100)$ compared with $O(1)$] and the associated numerical techniques are not applicable here.

The second class we may loosely describe as 'heavily constrained' dynamics, where a system, typically describing the evolution of a solid object, evolves subject to (possibly) many hundreds of constraints. For example, in robotics and computer gaming, the evolution of an arm, defined by several invariant lengths joined at pivot points $\mathbf{x}_i$, may be defined entirely by the motion of $\mathbf{x}_i$, each point mass being allowed to evolve independently according to Newton's equations, but subject to the conservation of internal lengths and (possibly) constraints on internal angles (e.g. Witkin 1997). A secondary area of importance is molecular dynamics, in which the evolution and structure of large molecules may be studied by evolving the requisite collection of atoms from an appropriate initial configuration. However, such systems are often stiff, that is, there is a large range of timescales that must be resolved, even if interest is only focussed on the slower dynamics. To eliminate short timescales, and therefore to increase the time over which the system may be evolved, it is common to fix various internal bond lengths and angles and thus supply a large number of constraints to the system (Ciccotti *et al.* 1982). For these dynamical systems, if the number of constraints is small, in principle one can construct a Lagrangian method in a generalized coordinate system in which the constraints are automatically satisfied. However, this is intractable in large systems and it is often expedient to consider a set of point masses that evolve subject to imposed invariants, achieved numerically principally using two methods. First, in the post-stabilization approach (Shampine 1986), the system of particles are evolved as if they were entirely independent. At the end of each time step, the state vector is perturbed by a small amount to ensure that the constraints are satisfied; if many such perturbations are possible, that which minimizes some given norm is typically chosen. One promising characteristic of this scheme is that it will always maintain the constraints exactly; however, there is, in general, no physically motivated choice of norm. The second method involves the imposition of time-dependent internal forces that, for instance, ensure that a set of internal lengths never change. These forces are chosen such that they do no work on the system and are therefore given as $\boldsymbol{\lambda}^T \mathbf{J}$, where $\mathbf{J} = \mathbf{dC}/\mathbf{dq}$ is the Jacobian of the constraints $\mathbf{C}$ with respect to the variables $\mathbf{q}$, and $\boldsymbol{\lambda}$ is a vector of Lagrange multipliers (Witkin 1997). Since $\mathbf{J}$ is known, all that remains is to find $\boldsymbol{\lambda}(t)$ in order that the constraints remain satisfied. This is typically achieved by imposing $\mathrm{d}^2\mathbf{C}/\mathrm{d}t^2 = \mathbf{0}$ and solving the resulting (linear) system (e.g. Baumgarte 1972).

The 'heavily constrained' class of problems bears the most similarity to Taylor's constraint. Not only are the number of constraints under consideration broadly comparable, but the role of $u_g(s)$ is similar to $\boldsymbol{\lambda}$ and, furthermore, both are given by a linear equation whose coefficients depend non-linearly on the state of the system. However, while $\boldsymbol{\lambda}$ can be determined through solving a simple linear matrix–vector system, $u_g(s)$ is defined by a second-order ordinary differential equation whose accurate solution is not easy to find, as we discussed.

The remainder of the paper is arranged as follows. In the next section, we discuss how to construct the local tangent plane and the projection $\mathcal{P}$, along with the associated computational details. Section 3 describes how Taylor's time-evolution scheme can be amended with the projection method along with several examples. In Section 4 we discuss the pros and cons of the projection method and end with general concluding remarks in Section 5.

2 CONSTRUCTION OF THE TANGENT PLANE

2.1 Finite characterization of Taylor's constraint

We discretize the (divergence-free) magnetic field in a truncated set of poloidal and toroidal vector spherical harmonics,

$$\mathbf{B} = \sum_{l=1}^{L_{\max}} \sum_{m=0}^{l} \left[\mathbf{S}_l^{m\,s/c} + \mathbf{T}_l^{m\,s/c} \right], \tag{7}$$

where

$$\mathbf{S}_l^{m\,s/c} = \boldsymbol{\nabla} \times \boldsymbol{\nabla} \times \left[Y_l^{m\,s/c}(\theta, \phi)\, S_l^{m\,s/c}(r)\, \hat{\mathbf{r}} \right],$$
$$\mathbf{T}_l^{m\,s/c} = \boldsymbol{\nabla} \times \left[Y_l^{m\,s/c}(\theta, \phi)\, T_l^{m\,s/c}(r)\, \hat{\mathbf{r}} \right], \tag{8}$$

in spherical polar coordinates (r, θ, ϕ). The notation $Y_l^{m\,s/c}$ represents a (Schmidt quasi-normalized) spherical harmonic of degree l, order m and azimuthal dependence $\sin m\phi$ or $\cos m\phi$ as appropriate. The superscript 's/c' will be dropped henceforth to simplify notation, except where we wish to draw attention to particular harmonics.

The development of the theory with which we can describe Taylor's constraint is much simplified in a full-sphere (with no solid inner core): the spherical shell case follows along similar but more involved lines. The magnetic field satisfies two key conditions: (i) it must be everywhere smooth (infinitely differentiable) including at the origin, and (ii) it is required to satisfy electrically insulating boundary conditions. We adopt a fully spectral representation in radius in terms of a Galerkin scheme of the form

$$S_l^m(r) = \sum_{n=1}^{N_{\max}} a_{lmn} S_{ln}(r), \qquad T_l^m(r) = \sum_{n=1}^{N_{\max}} b_{lmn} T_{ln}(r), \tag{9}$$

in which condition (i) is satisfied by restricting the two families of basis functions, $S_{ln}(r)$ and $T_{ln}(r)$, to be of the form

$$r^{l+1}\, Q_n(r^2) \tag{10}$$

where Q_n is a polynomial of degree n (e.g. Boyd 2001). Condition (ii) is equivalent to the requirement that

$$\frac{\mathrm{d}S_l^m(r)}{\mathrm{d}r} + l S_l^m(r) = 0, \qquad T_l^m(r) = 0, \tag{11}$$

which places simple linear constraints on the structure of Q_n. There remains some flexibility in selecting the Q_n; here, we choose them to render the basis sets, S_{ln} and T_{ln}, orthonormal:

$$\int_0^1 S_{ln}(r)\, S_{lk}(r)\, (1 - r^2)^{-1/2}\, \mathrm{d}r$$
$$= \int_0^1 T_{ln}(r)\, T_{lk}(r)\, (1 - r^2)^{-1/2}\, \mathrm{d}r = \delta_{nk}. \tag{12}$$

Each radial basis function behaves asymptotically like an individual one-sided Jacobi polynomial and therefore takes on many of the optimal properties of the Jacobi polynomials themselves (Li *et al.* 2010). As an alternative to this choice of orthonomality, by imposing orthogonality on derivatives of these functions rather than the functions themselves, it is often possible to quasi-diagonalize the representation of certain differential operators, for example, the Laplacian in spherical polar coordinates (Livermore 2010).

In the representation (9), it was shown in Livermore *et al.* (2008) that $\mathcal{T}(s)$ (of eq. 3) is simply

$$\mathcal{T}(s) = s^2 \sqrt{1 - s^2}\, \tilde{Q}_{L_{\max}+2N_{\max}-2}(s^2), \tag{13}$$

for some polynomial $\tilde{Q}_n$ of degree n. Thus, Taylor's constraint can be enforced (for every s in the continuum $0 \le s \le 1$) by requiring each polynomial coefficient to vanish (including the constant coefficient $s^0 = 1$). Because the magnetic field satisfies the insulating boundary conditions, it may be further shown that the polynomial coefficients in $\mathcal{T}(s)$ are linearly degenerate and the total number of constraints that must be satisfied is $\mathcal{C} = L_{\max} + 2N_{\max} - 2$. Each polynomial coefficient of $\tilde{Q}$ in $\mathcal{T}(s)$ is quadratic in the spectral coefficients of the magnetic field, (a_{lmn}, b_{lmn}), since $\mathcal{T}(s)$ is a quadratic functional of $\mathbf{B}$, and defines a set of constraints of significantly smaller size than the number of degrees of freedom $\mathcal{L} = 2\, L_{\max}\, (L_{\max} + 2)\, N_{\max} \gg \mathcal{C}$. That is, $O(N)$ constraints for $O(N^3)$ degrees of freedom where $N = N_{\max} = L_{\max}$. This is strongly suggestive of a very large solution space although, since the constraints are non-linear, little can be said rigourously about its size.

2.2 The tangent hyperplane to the Taylor manifold

Let us consider the general setting of a system of size $\mathcal{L}$ governed by the set of $\mathcal{C} \ll \mathcal{L}$ constraints

$$c_k(\mathbf{b}) = 0, \qquad k = 1, 2, 3, \ldots, \mathcal{C},$$

where $\mathbf{b}$ is a vector of spectral coefficients [here, of the magnetic field, $\mathbf{b} = (a_{lmn}, b_{lmn})$] and c_k are some non-linear functionals. In our case, c_k are quadratic, although the methodology of constructing the local tangent plane admits the generalized form.

Let us assume that both $\mathbf{b}$ and an infinitesimal perturbation of the form $\mathbf{b} + \delta\mathbf{b}$ lie on the manifold, where $\delta\mathbf{b}$ lies in the local tangent hyperplane to the manifold at $\mathbf{b}$. It is immediate that, to first order,

$$J\, \delta\mathbf{b} = \mathbf{0}, \tag{14}$$

where $J_{kj} = \partial c_k / \partial b_j$ is the Jacobian matrix of the constraints with respect to the spectral coefficients. Let us denote the kth row vector of J by $\mathbf{n}_k$ (i.e. $\mathbf{n}_k$ is the vector of derivatives of constraint c_k with respect to the spectral coefficients). Then $\delta\mathbf{b}$ is perpendicular to each $\mathbf{n}_k$ and thus the tangent hyperplane, spanned by all possible such $\delta\mathbf{b}$, is everywhere perpendicular to the $\mathbf{n}_k$. We now consider how to project any vector $\mathbf{v}$ onto the local tangent to the manifold, which is possible with only knowing the vectors normal to its surface. The projection is expedited if we first find an orthonormal set $\{\mathbf{q}_1, \mathbf{q}_2, \ldots \mathbf{q}_{\mathcal{C}}\}$ that spans the same space as $\{\mathbf{n}_1, \mathbf{n}_2, \ldots \mathbf{n}_{\mathcal{C}}\}$, which may be accomplished in principle by using a Gram–Schmidt procedure [although this is prone to numerical error (Press *et al.* 1992): a better suggestion is discussed below]. We then need to find α_i such that

$$\mathbf{q}_j^T \left(\mathbf{v} + \sum_{i=1}^{\mathcal{C}} \alpha_i \mathbf{q}_i \right) = 0, \qquad j = 1, 2, \ldots, \mathcal{C}, \tag{15}$$

that is, adding to $\mathbf{v}$ a certain combination of the normal vectors such that the result lies in the tangent plane. By orthonormality, it is immediate that $\alpha_i = -\mathbf{v} \cdot \mathbf{q}_i$. An interesting extension of this is not to seek the projection of $\mathbf{v}$ onto the tangent plane, but instead to consider the much more difficult problem of projecting $\mathbf{v}$ onto the (non-linear) manifold itself. One possible way of proceeding is to note that the axisymmetric toroidal harmonics appear only linearly in the quadratic Taylor constraints; assuming all other coefficients are prescribed, a linear solve places the solution exactly on the manifold (Livermore *et al.* 2009). However, this singles out a particular subset of harmonics and does not guarantee to perturb the solution by a distance that is minimal in any physically derived norm; that is, it may not project the vector $\mathbf{v}$ onto the 'closest' place on the

manifold. Motivated by the tangent plane methodology, one may be tempted to seek an intersection of a perturbation of the form $\mathbf{v}+\sum_{i=1}^{\mathcal{C}}\alpha_i\mathbf{q}_i$ with the Taylor manifold, with the belief that the normal directions to the local tangent plane would provide an optimal direction in which to search. This would require the solution of $\mathcal{C}$ coupled quadratic equations in $\mathcal{C}$ unknown values of α. Although the linearized version (15) is guaranteed in general to have a unique solution, this non-linear system does not: there may be more than one solution, or no solutions at all. In the latter eventuality, a more general search space would be required, although one would anticipate that any non-linear solution however obtained would lie close to the linearized solution. Thus, if an iterative approach was used to solve the non-linear system, the solution to (15) would constitute a good starting guess. Further discussion of non-linear schemes and their attendant complexities is not pursued here.

We now return to the tangent plane projection and discuss an alternative method of computing a set of orthonormal vectors. From (14) it is clear that $\delta\mathbf{b}$ must lie in the null-space of J and, since $\delta\mathbf{b}$ is an arbitrary vector in the tangent plane, the null-space of J defines the local tangent hyperplane at $\mathbf{b}$. We can then write J in singular value decomposition

$$J = U\,S\,V^T.$$

We may partition the row vectors of V^T (which are mutually orthogonal) into two classes: those lying within the tangent plane, and those perpendicular. We begin by defining a matrix Y whose rows are simply those rows of V^T corresponding to zero singular values in S. The rows of Y span the tangent hyperplane at $\mathbf{b}$ (i.e. the null-space of J) since, for any linear combination of such rows, pre-multiplication by J gives the zero vector. By orthonormality of V^T, it follows that all remaining rows (corresponding to non-zero singular values in S), which we may group into the matrix W, are perpendicular to the tangent plane. Indeed, pre-multiplication by J of any linear combination of these rows gives a non-zero vector and cannot reside within the tangent space. Note that the space spanned by the rows of W is also spanned by the set $\{\mathbf{q}_1, \mathbf{q}_2, \ldots \mathbf{q}_{\mathcal{C}}\}$. Consider multiplication of any vector $\mathbf{v}$ by Y^TY. If $\mathbf{v}$ is in the tangent plane then, by orthonormality of V, $Y^TY\mathbf{v} = \mathbf{v}$; if $\mathbf{v}$ lies orthogonal to the tangent plane then $Y^TY\mathbf{v} = \mathbf{0}$. Thus, multiplication by Y^TY projects any vector onto the tangent plane. Equivalently, multiplication by W^TW gives the projection orthogonal to the tangent plane, or $Y^TY = I - W^TW$. There are several remarks worth noting about the above method. First, compared to a Gram–Schmidt method, although at first sight perhaps more involved, the singular value decomposition allows a much more stable and accurate computation of a set of spanning normal vectors. Secondly, because of the relatively small number of constraints ($\mathcal{C} \ll \mathcal{L}$), for any vector $\mathbf{v}$, it is much more efficient to evaluate its projection using $(I - W^TW)\mathbf{v}$ than its equivalent form $Y^TY\mathbf{v}$. This is because we may exploit the fact that W has many fewer rows than Y and we can evaluate the projection as $\mathbf{v} - W^T(W\mathbf{v})$. Thirdly, since we need only to compute the matrix W rather than the whole matrix V, only the 'economy' singular value decomposition (SVD) decomposition is required.

Finally, we comment on the necessity of using a Galerkin radial scheme to construct the projection. At first sight, it might appear that any radial discretization would afford such a tangent-plane projection, but this is not so. Crucially, the Taylor manifold is defined by the intersection of those solutions that satisfy both (3) and (11). Any representation of the manifold (and therefore its tangent plane) must take both of these conditions into account. As a first example, consider a finite difference scheme. At the present time, this must be ruled out as the finite characterization of Taylor's constraint is only currently known for fully spectral radial schemes. A second alternative that we might have considered is a spectral scheme of 'Chebyshev-tau' type (e.g. Boyd 2001), where the toroidal and poloidal scalar functions are expanded in terms of (say, N) smooth basis functions that do not, individually, satisfy the boundary conditions. If two boundary conditions (11) are imposed, then typically the first $N-2$ coefficients are determined using the dynamics of the system, the final two coefficients by (11). Within the space defined by the first $N-2$ basis functions, we may form a projection onto the Taylor manifold as before. However, the problem remaining is that, after applying this projection, the modification to the magnetic field by the addition of the extra two spectral coefficients to fulfill (11) will violate Taylor's constraint. Crucially, the boundary conditions and the projection need to be imposed at the same time; this is currently possible only within a Galerkin scheme, for which an optimal theory has only recently been developed (Livermore 2010).

2.3 Computational considerations

We now apply the concepts developed to the specific problem of Taylor's condition, which requires rendering zero the polynomial form (13). Numerically, this may be achieved in many different ways, for instance, by considering the two equivalent monomial or Chebyshev representations:

$$\text{(i)}\quad \mathcal{T}(s) = s^2\sqrt{1-s^2}\sum_{k=0}^{K} c_k\, s^{2k}, \qquad \text{or}$$

$$\text{(ii)}\quad \mathcal{T}(s) = s^2\sqrt{1-s^2}\sum_{k=0}^{K} \tilde{c}_k\, T_{2k}(s), \tag{16}$$

or indeed by replacing the Chebyshev polynomials $T_n(s)$ above by any other spanning set of polynomials (e.g. any Jacobi polynomial). The range of k bounded above by $K = L_{\max} + 2N_{\max} - 3$ takes into account the linear degeneracy caused by the boundary conditions. The coefficients $\tilde{c}_k$ are simply a homogeneous linear combination of the c_k (reflecting the fact that the polynomials they multiply span the same finite subspace as the monomials). Therefore, to arrange that Taylor's condition is satisfied, we can choose either to set each c_k or each $\tilde{c}_k$ to zero. Formally (and in exact arithmetic), these two cases are equivalent, although in finite precision the resulting accuracy will differ as discussed below.

Each coefficient c_k or $\tilde{c}_k$ is exactly quadratic in the magnetic field coefficients and may be written

$$c_k = \sum_{i<j} T_{ijk}\, b_i\, b_j, \qquad \tilde{c}_k = \sum_{i<j} \tilde{T}_{ijk}\, b_i\, b_j. \tag{17}$$

We denote as the *Taylor tensor*[2] both T_{ijk} and $\tilde{T}_{ijk}$. Henceforth we shall refer to a general tensor T, where the context will make it clear which representation, either (i) elementary monomials or (ii) Chebyshev polynomials we refer to.

The Taylor tensor contains $\mathcal{L}^2\,\mathcal{C}$ elements, although is sparse, containing a non-zero entry T_{ijk} only if the spherical harmonics i and j 'interact', which requires specific selection rules to be satisfied (Livermore *et al.* 2008). The (symmetric) Taylor interaction is

[2] Strictly speaking a tensor is required to obey certain rules regarding transformations of the coordinate system which are not relevant here. However, the entries of the tensor are not arbitrary: clearly the two representations T_{ijk} and $\tilde{T}_{ijk}$ are related by a linear transformation and denotation as 'tensor' rather than 'array' or 'matrix' reflects this property.

Table 1. Summary of numerical parameters for a variety of truncations in spherical harmonic degree ($L_{\max}$) and in radius ($N_{\max}$). From left to right: the number of variables $\mathcal{L} = 2N_{\max} L_{\max} (L_{\max} + 2)$ in the spectral expansion, the number of Taylor constraints $\mathcal{C}$ in a full sphere, the number of non-zero elements *NNZ* of T for both monomial (M) and Chebyshev polynomial (C) representation indicated by superscripts. The rightmost two columns supply, correct to two significant figures, the density (the percentage of elements of T that are non-zero) and storage requirements (in double precision), both only for the Chebyshev presentation, this being the most expedient choice as discussed in the text. A formula to enumerate both NNZ^{M} and NNZ^{C} is given and briefly proved in the Appendix.

$L_{\max}$	$N_{\max}$	$\mathcal{L}$	$\mathcal{C}$	NNZ^{M}	NNZ^{C}	Density$^{\mathrm{C}}$ (per cent)	Storage$^{\mathrm{C}}$/Mb
6	4	384	12	20 754	23 414	1.7	0.18
8	6	960	18	146 694	167 358	0.88	1.3
10	6	1440	20	299 406	351 876	0.72	2.7
12	4	1344	18	199 182	248 374	0.61	1.9
12	6	2016	22	542 502	654 042	0.61	5.0
14	8	3584	28	1 867 634	2 242 554	0.52	17
20	10	8800	38	10 722 486	13 236 186	0.36	100
50	20	104 000	88	1 373 887 706	1 781 641 206	0.14	13 000

defined by

$$[\mathbf{B}_i, \mathbf{B}_j] = \int_{C(s)} \left([\nabla \times \mathbf{B}_i] \times \mathbf{B}_j\right)_\phi s \, \mathrm{d}\phi \, \mathrm{d}z + \int_{C(s)} \left([\nabla \times \mathbf{B}_j] \times \mathbf{B}_i\right)_\phi s \, \mathrm{d}\phi \, \mathrm{d}z, \tag{18}$$

where $\mathbf{B}_i$ and $\mathbf{B}_j$ are two magnetic fields. Note that the contributions of each of the two terms above are not individually symmetric under interchange of i and j (see eqs 2.7–2.9 in Livermore *et al.* 2008). A natural way to represent T_{ijk} is a symmetric quadratic form; we therefore need only store one of the two symmetric halves, or equivalently write T_{ijk} in a strictly upper triangular format [hence the restriction $i < j$ in eq. (17)]. To exploit the sparsity when computing $\mathcal{T}(s)$ (or any derived quantities), we could attempt to derive the form of any banded structures in the tensor and create a one-to-one map of the non-zero entries to a dense vector of coefficients. However, as illustrated later, the structure of the tensor is highly complex and such a task is far from trivial. Instead, we proceed more directly and create an ordered list of the form

$$[i, j, k, T_{ijk}],$$

which gives, in ascending order in i, only those harmonics $j > i$ that give a non-zero contribution to T_{ijk}. Of particular note is that the matrix J given by

$$J_{kl} = \frac{\partial}{\partial b_l} \sum_{i<j} T_{ijk} \, b_i \, b_j = \sum_{i<l, l<j} (T_{ilk} + T_{ljk}) \, b_l \tag{19}$$

can be efficiently computed by taking one row at a time of the list representation of T and computing its contribution to the two relevant entries in J. The elements of T are evaluated analytically using computer algebra (with the package Maple) and written to disk in double precision floating point format.

Table 1 shows a summary of the numerical parameters involved for various truncations in spherical harmonic degree ($L_{\max}$) and in radius ($N_{\max}$). The number of magnetic field spectral coefficients is denoted $\mathcal{L}$ and the number of Taylor conditions as $\mathcal{C}$. As noted, the Taylor tensor is very sparse, as indicated by the number (NNZ) and fraction of non-zero elements. The superscript in the column heading denotes whether monomials (M) or Chebyshev polynomials (C) are used in the representation of Taylor tensor. A formula for NNZ is given and briefly proved in the Appendix.

To further illustrate the sparsity of the Taylor tensor and highlight its structural complexity, Fig. 3 shows a graphical depiction as 2-D symmetric matrices. Adopting the truncation $L_{\max} = 8$, $N_{\max} = 6$ associated with 960 spectral coefficients, a corresponding 960 × 960 grid contains a black dot at the (i, j) entry if T_{ijk} or T_{jik} is

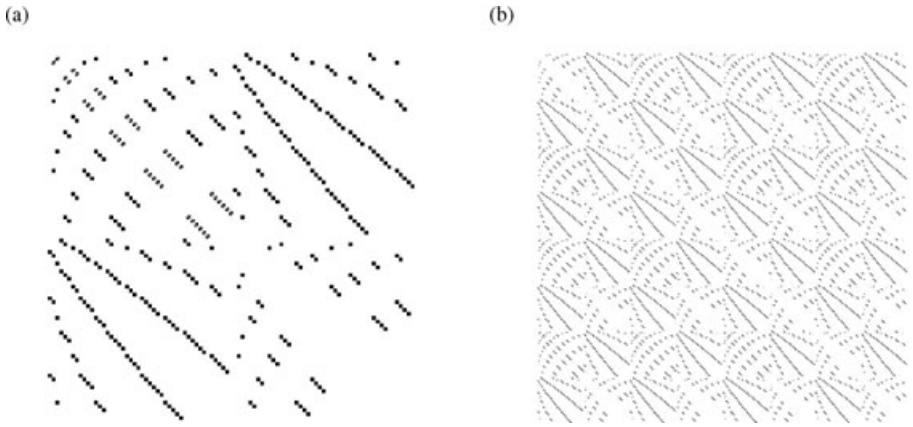

Figure 3. Graphical representation of the sparsity and structure of the Taylor tensor in terms of a 2-D projection $\xi_{ij} = \max_k f(T_{ijk})$, where $f(x) = 1$ if $x \neq 0$ and zero otherwise, at truncation $L_{\max} = 8$, $N_{\max} = 6$. In each 960 × 960 matrix, $\xi(i, j)$ is coloured black if it takes the value 1 (equivalent to the condition that the harmonics i and j (or j and i) have a non-zero interaction) or is coloured white otherwise. Matrix (a) is defined in terms of the spectral ordering where the radial index varies most rapidly; this produces large blocks (rather than points). Matrix (b) adopts the spectral ordering where the harmonic index varies the fastest. Both (a) and (b) contain the same number of black dots in highly complex structures, each having an associated Taylor-tensor density of 0.88 per cent.

non-zero for any k (i.e. harmonics i and j interact); the position is coloured white otherwise. Such a matrix is independent of the representation used to formulate the Taylor tensor, since we are only concerned with non-zero interactions and not their expansion in any particular set of polynomials. The only remaining issue is to decide how the spectral coefficients are ordered. There are two natural ways of doing this; common to each is an ordered list of the spherical harmonics within the truncation $0 \le m \le l \le L_{\max}$ of size $N = 2L_{\max}(L_{\max} + 2)$, distinguishing between poloidal and toroidal types. In Fig. 3(a), consistent with the results in Section 3.3, the spectral coefficients are ordered as $((i, n)_{n=1,2,\ldots,N_{\max}})_{i=1,2,\ldots,N}$, where i indicates the harmonic index and n the radial index; that is, the radial index varies most rapidly. This produces large blocks of interactions in the image. In Fig. 3(b), the order is the opposite: $((i, n)_{i=1,2,\ldots,N})_{n=1,2,\ldots,N_{\max}}$, that is, with the radial index varying most slowly. This has the effect of spreading out the interactions and creating a more scattered image. However, as they represent the same object, both (a) and (b) have the same number of black dots. It is clear that the structure is extremely complex, and that producing an analytic mapping of the grid position (i, j) to locate the non-zero entries is a highly non-trivial task.

Finally, we briefly discuss why we have troubled to introduce different representations for the Taylor tensor (given that they are formally equivalent); in particular, why there is an optimal choice from numerical considerations. The computation of J, required to compute the normals to the tangent plane, necessitates the contraction of T with the vector of coefficients $\mathbf{b}$ (19). In fixed precision, severe inaccuracies can arise if the quantities to be added vary dramatically in magnitude, due solely to roundoff error. For this reason, it is expedient to find a representation of T with its elements of minimal range in magnitude. As a starting point for a discussion, Fig. 4 shows coefficients taken from two representations of the Taylor tensor given by the interaction between the axisymmetric harmonics: toroidal; $l = 9$; $n = 6$ (harmonic i) and poloidal; $l = 10$, $n = 6$ (harmonic j). With k plotted in the horizontal direction, the monomial coefficients T_{ijk} are depicted by circles and the Chebyshev coefficients $\tilde{T}_{ijk}$ by diamonds. It is immediately apparent that the entries of T_{ijk} vary by $O(10^{10})$, whereas those of $\tilde{T}_{ijk}$ vary by only $O(10^2)$. Thus, the Chebyshev representation offers much better

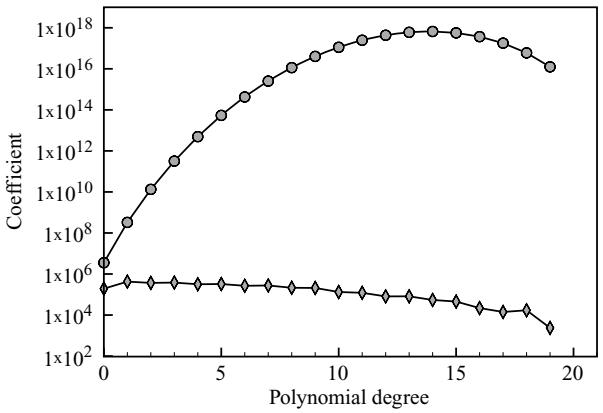

Figure 4. A comparison of representations of the Taylor interaction between the axisymmetric toroidal $l = 9$, $n = 6$ magnetic field mode and the axisymmetric poloidal $l = 10$ $n = 6$ mode. The circles show the spectral coefficients (c_k) and diamonds the Chebyshev coefficients $\tilde{c}_k$. The range of coefficients are much greater for the monomial representation than the Chebyshev case and the latter is therefore numerically preferred for constructing the tangent plane.

alternative to the monomial representation, a result confirmed by the time-dependent calculations in Section 3.3. Of all possible orthogonal polynomials, whether or not the Chebyshev polynomials in particular offer an optimal representation we cannot say; but we speculate, owing to their uniform oscillation property, that they are close to it. Furthermore, it is likely that any optimal representation depends on the structure of the magnetic field modes: in particular, the choice of radial basis functions and, to a similar extent, the basis functions in solid angle too (here being the spherical harmonics).

3 IMPROVING TAYLOR'S ALGORITHM USING PROJECTION

3.1 An improved algorithm

Having all ingredients now in hand, we now show how the projection method may be implemented. We discretize (1) and (2) by adopting a standard spherical harmonic representation (as described in Section 2.1) for both the flow and magnetic field; the equations are then projected back onto the basis using de-aliased transforms (e.g. Hollerbach 2000). The projection method, described in the previous section, may be added onto Taylor's algorithm to produce a refined estimate of the rate of change of magnetic field. After finding (a possibly inaccurate) estimate of $\mathbf{u}$ and then computing the (approximate) discretized form of the right-hand side of (2), written here as $f(\mathbf{b})$, we may find the projection onto the local tangent space, $\mathcal{P}_{\mathbf{b}} f(\mathbf{b})$, by the following procedure:

Compute $J_{kj} = \sum (T_{ijk} + T_{jik})\, b_j$
$[U, S, V^T] = \mathrm{svd}(J, \mathrm{economy})$
Form W from V
$\mathcal{P}_{\mathbf{b}}(f(\mathbf{b})) = \left(\mathbf{v} - W^T W f(\mathbf{b})\right)$

The modified discretization of the induction equation we now want to evolve is

$$\frac{\partial \mathbf{b}}{\partial t} = \mathcal{P}_{\mathbf{b}}(f(\mathbf{b})),$$

to which we may now apply any time-stepping scheme; for this initial study, we adopt a standard Runge–Kutta scheme of order four. It is worth noting explicitly that although f, above, is a discretization of a linear operator (and so, notwithstanding truncation errors, is linear), when coupled with the projection operator, this first-order partial differential equation becomes inherently spatially non-linear.

In terms of computational expense, the requirement to compute $\mathcal{P}$ with every evaluation of $\mathbf{f}(\mathbf{b})$ is very costly. The majority of computational effort is taken up by the evaluation of the matrix J which takes $O(L_{\max}^6)$ operations (if $L_{\max} = N_{\max}$, see the Appendix) compared to only $O(L_{\max}^4)$ for any slow transform (such as the Legendre transform in colatitude or radial transform via quadrature). However, this can be speeded up significantly using a parallel computation. The evaluation of the singular value decomposition itself by comparison is relatively very fast, as tests show, although if required it could be speeded up by linearization about a previous state (Liu *et al.* 2008).

To evaluate how close the evolving magnetic field is to the Taylor manifold, we use two non-dimensional measures of 'Taylorization'. The first is elementary to compute (within the framework already described) and defines departures from the manifold in spectral space: it is defined as

$$\sigma = \frac{\sum_{i=1}^{\mathcal{C}} |\tilde{c}_k|}{\mathcal{C} \int_V \mathbf{B}^2 \, \mathrm{d}V},$$

where $\tilde{c}_k$ are defined in (17). Note that this measure is representation specific (we could equally well define it using c_k), and that each $\tilde{c}_k$ is quadratic in $\mathbf{B}$ and so σ is dimensionless (recall that length has already been non-dimensionalized).

The second is more physically motivated (and more standard in the literature) and is defined to be the rms measure

$$\tau = \sqrt{\frac{\int_0^1 \left[\int_{C(s)} \left([\nabla \times \mathbf{B}] \times \mathbf{B}\right)_\phi \, s \, \mathrm{d}\phi \, \mathrm{d}z\right]^2 \mathrm{d}s}{\int_0^1 \int_{C(s)} \left[\left([\nabla \times \mathbf{B}] \times \mathbf{B}\right)_\phi \, s\right]^2 \mathrm{d}\phi \, \mathrm{d}z \, \mathrm{d}s}}, \tag{20}$$

where $C(s)$ is a geostrophic cylinder at radius s. These two norms offer completely independent checks that a solution is on the Taylor manifold. The evaluation of σ is performed in Matlab simply by contracting the vector of magnetic field coefficients with relevant tensors and matrices all pre-computed in Maple. The Taylorization τ is computed numerically in Fortran 90 using Gauss and Gauss–Chebyshev quadrature. The computation of both σ and τ is exact apart from the rounding errors inherent in double precision.

3.2 An example magnetostrophic system: taking a few time steps

We will now illustrate the key issues by evolving a quasi-magnetostrophic system by a few time steps. Because the numerical tools to solve for $\mathbf{u}_{\rm mag}(\mathbf{B}, T)$ in general have not yet been properly developed, we cannot solve the full magnetostrophic system. Instead, by choosing a simple initial magnetic field, in the absence of buoyancy forces, we can find analytically the solution for $\mathbf{u}_{\rm mag}$ which we assume is constant for the 10 short time steps of length $h = 10^{-5}$ that we shall take. This is, of course, an approximation, but since the evolution time is short, the energy of $\mathbf{B}$ changes only by less than 1 per cent over these 10 time steps and a concomitantly small change in $\mathbf{u}_{\rm mag}$ would be expected. Within this simple example, the flow is driven entirely by the Lorentz force, and would represent the evolution of the geodynamo should the buoyancy force be suddenly turned off.

The following algorithm summarizes, given $\mathbf{B}(t_n)$, in this numerical experiment how we compute its rate of change:

1. Find $u_g(t_n) = u_g(\mathbf{u}_{\rm mag}, \mathbf{B}(t_n))$
2. $\mathbf{u}(t_n) = \mathbf{u}_{\rm mag} + u_g(t_n)\,\hat{\phi}$
3. Compute $\frac{\partial \mathbf{B}}{\partial t}$ from eq. (2); project back onto the spectral basis.

4*. Project onto tangent plane of manifold

Central to this exercise is to compare the above algorithm with, and without, step 4; that is, what happens if we follow Taylor's original algorithm compared to adding in projection. We will therefore compare the evolution of $\mathbf{B}$ or, more specifically, its Taylorization, which is evolved using a standard Runge–Kutta scheme of order four.

We will take the initial magnetic field to be

$$\mathbf{B}(t_0) = \lambda \, \nabla \times \nabla \times \left(Y_2^0 \, S_{2,1}(r)\, \hat{\mathbf{r}}\right)$$

corresponding to the $l = 2$, $m = 0$ poloidal mode of largest radial scale, following the notation of Section 2.1; λ is chosen so that $\mathbf{B}(t_0)$ has unit rms over the full sphere. If $T = 0$ (i.e. no buoyancy force) then the magnetostrophic flow is

$$\mathbf{u}_{\rm mag} = -\frac{1575\, r \sin\theta}{416} \left(-9 + 24\, r^2 - 15\, r^4 - 10\, r^2 \cos^2\theta + 10\, r^4 \cos^2\theta\right) \hat{\phi},$$

a colatitudinally dependent toroidal flow of spherical harmonic degree 3, containing only an azimuthal component. Note that, for numerical expediency, we have deliberately chosen an equatorially symmetric, axisymmetric initial field; for then $\mathbf{u}$ is also of this symmetry and it follows that $\mathbf{B}$ will remain, for all time, in this restrictive symmetry class. This reduces the computational workload, and allows us to work within the symbolic package Maple, allowing us to mix exact analytical procedures [in particular, to compute $G(s)$ of (5)] with numerical calculations. We shall use the spectral truncation $L_{\rm max} = 6$ and $N_{\rm max} = 4$ bearing in mind that we need only consider the poloidal modes of even degree and toroidal modes of odd degree, these being equatorially symmetric; barring degeneracies, the number of Taylor constraints is 12.

To find u_g, we write

$$u_g(s) = s \sum_{n=0}^{N-1} a_n \, T_n(2s^2 - 1) = s \sum_{n=0}^{N-1} a_n \, T_{2n}(s),$$

as a Chebyshev expansion truncated at N coefficients, exploiting the fact that it is known to be an odd function of s (Livermore *et al.* 2008). We now substitute this form directly into (5) and form a matrix system by evaluating at a set of collocation points, which we take to be the $N - 1$ zeros of $T_{N-1}(2s^2 - 1)$. There is some flexibility in the choice of collocation points, but this particular set can be justified as by using all the zeros of the given polynomial we have a 'uniform' resolution over [0, 1]. As an alternative, for example, we could use the smallest $N - 1$ (positive) zeros of $T_K(2s^2 - 1)$ for any $K > N$; however, the neglect of collocation points near $s = 1$ may limit convergence there. The linear system is completed by imposing the condition of zero total angular momentum about the rotation axis; that is, requiring that the angular momentum imparted from u_g exactly cancels out the angular momentum of $\frac{40\pi}{39}$ stemming from $\mathbf{u}_{\rm mag}$.

Before showing what happens during the evolution, it is instructive to compute the initial u_g to high accuracy. In Section 1.2 we discussed problems with finding accurate solutions to u_g, arguments that we illustrate here. Fig. 5(a) shows the spectrum of $|a_n|$ on a log–log plot as a function of index n when $N = 80$. At least over the range plotted, the convergence appears to follow the algebraic scaling n^{-1}, rather than exponential. The super-algebraic fall-off towards the right-hand end of the spectrum is not a converged feature. Two orders of magnitude decrease in the magnitude of the spectral coefficients requires an expansion up to index 20: that is, Chebyshev degree 40. This slow convergence is representative of the general case, and comes about due to the spatially varying (time-dependent) coefficient $\alpha(s)$ which multiplies the highest derivative in (5).

Fixing the time step as $h = 10^{-5}$, we now take 10 time steps with, and without, projection (using the Chebyshev representation for the Taylor tensor). When computing the projection, we must decide which singular values of J are zero and which are not. This is not as straightforward as it sounds: due to numerical imprecision, in general no *exact* zero singular values will arise. In a typical case we would calculate a subset of singular values all around the same magnitude, in addition to a remaining subset of much lower magnitude (which, would, in exact precision, be zero). Numerically we have to decide where the threshold lies that separates these two sets. For the calculations here, the largest singular values are $O(10^3)$ and we set the threshold as 10^{-7}.

Fig. 5(b) compares the evolution of the initial exact Taylor state, measured by the Taylorization σ (based on the Chebyshev representation). To evolve the magnetic field, all terms of the induction eq. (2) are present in the model, although $\mathbf{u}_{\rm mag}$ is held fixed. Of

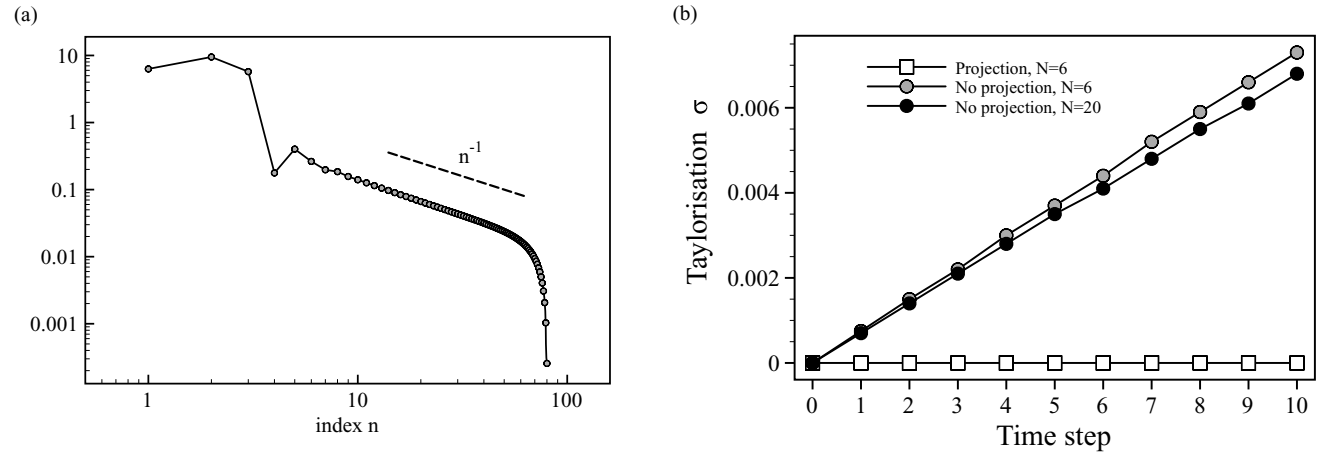

Figure 5. (a) For the initial magnetic field given in the text, convergence of the spectrum of u_g as a function of index n of the numerical approximation $u_g = s\sum_{n=0}^{N-1} a_n\, T_n(2s^2 - 1)$ shown as filled circles. On the range plotted, the convergence appears to be only algebraic, scaling as n^{-1}, giving rise to numerical problems in accurately representing u_g. The super-algebraic fall-off towards the right-hand end of the spectrum is not a converged feature. A spectral fall-off of two orders of magnitude requires a representation in (odd) Chebyshev polynomials of degree 40. (b) A comparison of the evolution of the induction equation system (described in Section 3.2) over 10 time steps of size $h = 10^{-5}$, with and without projection, measured by the Taylorization σ. Without projection, σ increases linearly with time and the solution rapidly leaves the manifold. Increasing N from 6 to 20 decreases the rate of divergence from the manifold only marginally. With projection, $\sigma = O(10^{-8})$ and increases only very slowly with time. The truncation used here is $L_{\max} = 6$, $N_{\max} = 4$; in the Legend, N is defined as in (a).

principal note is that, without projection, the Taylorization apparently increases linearly with time and will quickly leave the manifold (as shown by the circle symbols using resolutions $N = 6$ and $N = 20$). That σ increases with time in this manner can be easily seen by linearization; if $\mathbf{B}(t_1) = \mathbf{B}(t_0) + h\,\tilde{\mathbf{B}}$ where $\mathbf{B}(t_0)$ satisfies Taylor's constraint but $\mathbf{B}(t_1)$ does not, then after a single time step $\sigma(t_1) = 0 + h\,C(\mathbf{B}(t_0), \tilde{\mathbf{B}}) + O(h^2)$, where C is some constant [dependent on $\mathbf{B}(t_0)$ and $\tilde{\mathbf{B}}$]. Further time steps appear to add to this error, linear to leading order.

Fig. 5(b) also shows that, following Taylor's original algorithm, increasing N from 6 to 20 only decreases $\sigma(t)$ in a minor way. The reason for this (as discussed in Section 1.2) is simply that although u_g is represented to modest accuracy, the projection of the right-hand side of (2) back onto the basis set truncated at $L_{\max} = 6$, $N_{\max} = 4$ introduces a significant discretization error for the action of u_g. This can be identified most easily for the initial time step. Since $\mathbf{B}(t_0)$ is of spherical harmonic degree 2, then almost all of the spectral-tail of u_g, containing spherical harmonic degrees higher than 8, induces no field of degree less than six (see the selection rules of Bullard & Gellman 1954); thus the truncation procedure ignores the spectral tail of u_g and effectively reduces its resolution.

The square data points in Fig. 5(b) give the Taylorization when using the projection method with $N = 6$. On this linear scale (chosen to show the linear divergence of the non-projection method from the manifold), the Taylorization $\sigma(t)$ is graphically indistinguishable from zero. It is, in fact, $O(10^{-8})$, and increases only very slowly with time (in fact, after a single step, $\sigma(t_1) = O(10^{-8})$ and it only increases with increments of $O(10^{-11})$ for every time step thereafter). The cases of $N = 6$ and $N = 20$ (not shown) give very similar behaviour, owing to the fact that the projection algorithm ensures the evolution of $\mathbf{B}$ is tangent to the Taylor manifold, irrespective of the accuracy of u_g. The non-uniform behaviour of σ in time suggests that there is something very special about the geometry of the manifold at the particular initial condition we have chosen of a single, axisymmetric, harmonic, which leads to a minor degradation in accuracy during the first time step. Such an issue will not influence the general case however: when evolving a magnetic field of no particular symmetry as described in the following section, we find no such behaviour.

3.3 The importance of the choice of Taylor tensor

The previous example illustrated some of the key aspects inherent in evolving a magnetostrophic system, albeit for a small number of time steps. By adopting an even simpler case that may be treated exclusively numerically, we now present some more results on the projection algorithm. Specifically, although anticipated by the discussion in Section 2.3, we will investigate the numerical issue of whether or not the Chebyshev representation of the Taylor tensor is really superior to the monomial representation. Furthermore, we will be able to test the accuracy of the evolution algorithm for a system evolved for many more time steps than before.

Our model contains only the basic ingredients of some vector $\mathbf{f}$, representing an approximation to $\frac{\partial \mathbf{B}}{\partial t}$, and the projection method to confine the evolution to the manifold.

$$\frac{\partial \mathbf{b}}{\partial t} = \mathcal{P}_{\mathbf{b}}\left[\mathbf{f}\right]. \tag{21}$$

Perhaps the simplest example would be to choose $\mathbf{f}$ to be constant (in time) and to then test how well Taylor's constraint is maintained. However, we use

$$\mathbf{f} = \nabla^2 \mathbf{B},$$

which exhibits more complex $\mathbf{B}$-dependence. Physically, this may be viewed as evolving the magnetic diffusion equation subject to Taylor's constraint.

Since we are no longer confined to axisymmetry, we adopt an initial magnetic configuration that is much more general than that used before: having energy in all wavenumbers. We use the method described in Livermore *et al.* (2009), in which we exploit the fact that the axisymmetric toroidal coefficients never themselves appear as squared terms in the Taylor constraints c_k. By assuming that all the remaining coefficients are prescribed, we only need to solve a linear system to find an exact Taylor state, rather than having to

Table 2. A comparison of two methods of computing the tangent plane and the Taylorization that results, for a variety of spatial truncations, in our simple projection model. For either the monomial or Chebyshev representation of the Taylor tensor, the rows are listed in order of problem complexity, judged by the the number of degrees of freedom $\mathcal{L}$ and the number of constraints $\mathcal{C}$. The fifth column gives the initial value of τ. Columns 6–10 show τ_n, the Taylorization at the end of the time interval [0, 0.01] having taken n equal time steps using a Runge–Kutta scheme of order 4. In each case the Chebyshev representation supplies a much more accurate Taylor state for an initial condition. At low resolutions both methods then behave comparably for the time-evolution problem. However, at larger truncations the Chebyshev representation is superior enabling a much more accurate Taylorization to be maintained.

$L_{\max}$	$N_{\max}$	$\mathcal{L}$	$\mathcal{C}$	τ_{init}	τ_{10}	τ_{100}	τ_{1000}	$\tau_{10\,000}$	$\tau_{100\,000}$
Monomial representation									
6	4	384	12	5.4e-12	3.0e-1	7.8e-5	3.1e-9	2.9e-11	1.2e-11
8	6	960	18	5.5e-9	6.6e-1	3.7e-3	5.1e-5	9.8e-8	1.7e-7
12	4	1344	18	8.6e-10	2.2e-1	7.9e-5	1.5e-7	2.3e-7	1.1e-7
10	6	1440	20	5.4e-8	4.6e-1	5.5e-2	1.1e-4	3.6e-5	1.6e-5
10	8	1920	24	1.5e-7	6.8e-1	1.9e-1	4.2e-2	3.6e-2	3.8e-2
Chebyshev polynomial representation									
6	4	384	12	4.3e-14	3.0e-1	7.8e-5	3.1e-9	2.9e-11	1.2e-11
8	6	960	18	2.1e-12	6.6e-1	3.7e-3	5.1e-5	6.9e-10	3.9e-11
12	4	1344	18	3.4e-12	2.2e-1	7.9e-5	4.4e-9	2.9e-11	3.0e-11
10	6	1440	20	8.3e-14	4.6e-1	5.5e-2	4.0e-6	3.2e-10	3.2e-10
10	8	1920	24	3.4e-11	7.0e-1	2.0e-1	5.9e-5	4.0e-9	1.6e-9

solve a set of coupled quadratic equations. To avoid any particular symmetries, our approach is to fill each non-axisymmetric-toroidal entry of the vector **b** with pseudo-random values drawn from the interval [0, 1] that are shaped with the envelope $e^{-(l+n)/2}$ to mimic an exponential fall-off with (l, n). The remaining set of axisymmetric toroidal modes are larger in number than the number of constraints $\mathcal{C}$ and, in principle, we may select any $\mathcal{C}$ of them to formulate a linear system. However, some choices lead to poorly conditioned linear systems and inaccurate Taylor states. Our approach was to select the first $\mathcal{C}$ modes from the ordered list (l, n) where both l and n decrease from ($L_{\max}$, $N_{\max}$) with l varying most quickly. The results of this procedure were generally excellent (see column 5 of Table 2), producing an extremely small Taylorization $\tau = O(10^{-11})$ or better, using the Chebyshev representation of the Taylor tensor. The monomial representation did not behave so well, since its linear system was more poorly conditioned, and produced $\tau = O(10^{-7})$ or better. The remarks noted in Livermore *et al.* (2009) of potential problems in computing accurate Taylor states (with the monomial representation in mind) are now greatly offset by the high performance of the Chebyshev representation.

Consider the same moderate truncation as before: $L_{\max} = 6$, $N_{\max} = 4$, in which 384 variables must be evolved with 12 Taylor constraints. Using the Chebyshev representation, we evolve the initial condition from $t = 0$ until $t = 0.01$ in 1000 steps of size $h = 10^{-5}$. The end time corresponds to around 1/10 of the so-called 'dipole diffusion time' ($1/\pi^2$ in our dimensionless units), corresponding to the slowest free decay time of the full-sphere system $\frac{\partial \mathbf{B}}{\partial t} = \nabla^2 \mathbf{B}$. Fig. 6 shows the evolution quantified in terms of the measures of Taylorization σ and τ. There are two key features of note. First is that the measures are very similar in magnitude and time-dependence, thus each is an excellent proxy for the other. This also confirms that our calculations are correct because, as previously noted, σ and τ are computed using completely different techniques. Second is that both measures of Taylorization are $O(10^{-8}) - O(10^{-11})$, very much smaller than 1.

Comparable calculations using different resolutions and time steps h, for both the Chebyshev and monomial representation, are shown in Table 2. For each representation, the runs are listed in order of problem complexity as judged by the number of degrees of freedom $\mathcal{L}$ and the number of constraints $\mathcal{C}$. In the fifth column is the value of τ, a measure of the Taylorization, for the initial field. In columns 6–10 are shown, τ_n, the value of τ at the end of the time interval [0, 0.01] after taking n equal time steps of size h. At low resolution (e.g. $L_{\max} = 6$, $N_{\max} = 4$), aside from the initial condition (which we have already remarked upon), the Chebyshev and monomial representations behave identically. Furthermore, they produce values of τ_{10}, τ_{100} and τ_{1000} which decrease by a factor of 10^4 each time, in agreement with the $O(h^4)$ accuracy of the Runge–Kutta scheme, although this property is apparently not obeyed for smaller time steps in this example (presumably due to roundoff error in double precision) and for higher truncations. For this lowest resolution example, errors induced by ill-conditioning of the Taylor tensor apparently have no effect (the truncation not being sufficiently high to expose their influence) and accuracy is limited only by computational roundoff errors at $O(10^{-11})$. However, at the largest

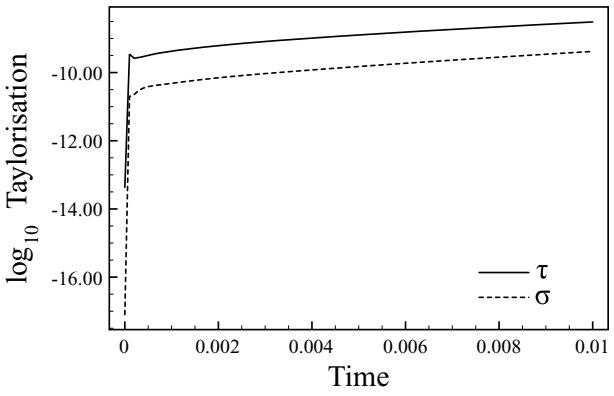

Figure 6. Time evolution of two different (non-dimensional) measures of Taylorization: σ (using the Chebyshev representation) and τ. Both measures behave similarly and lie in the range $O(10^{-8}) - O(10^{-11})$, although in this example σ is around one order of magnitude smaller than τ.

truncations shown, the situation is reversed. The monomial representation becomes increasingly ill-conditioned and behaves poorly: at $L_{\max} = 10$, $N_{\max} = 8$, τ (at $t = 0.01$) cannot be rendered smaller than $O(10^{-2})$ even at the smallest value of h shown. Indeed, by comparing the values of $\tau_{10\,000}$ and $\tau_{100\,000}$ it would appear that subsequent decreases in the time step would serve only to increase, rather than decrease τ. That is, computational roundoff errors vastly exacerbated by the poor monomial representation swamp the solution and prevent convergence in h to a solution evolving on the Taylor manifold. In contrast the Chebyshev representation performs very well, even in the same highest resolution example, it being possible to maintain a Taylorization $\tau = O(10^{-9})$ for the two smallest values of h considered. In this case, improved conditioning ensures that computational roundoff errors do not prevent convergence to highly accurate solutions.

For comparison with existing estimates in the literature of geodynamos at small Ekman number, both Rotvig & Jones (2002) and Stellmach & Hansen (2004) calculated $\tau = O(10^{-1}) - O(10^{-2})$ (note that the Taylorization defined in Rotvig & Jones (2002) is analogous to our τ^2). It is clear that our numerical method is able to satisfy Taylor's constraint to a much higher precision.

Finally, we note that the calculations up to $t = 0.01$ are apparently stable; further calculations indicate that this stability is maintained at least up to $t = 0.1$, and probably indefinitely. However, we remark that the value of τ for the constrained problem does in fact keep increasing for times beyond $t = 0.01$. In fact, at $t = 0.1$, it has risen to $O(10^{-6})$. Although this is still small, it highlights the fact that, due to numerical error, eventually the solution will indeed diverge from the manifold (albeit very slowly); this is discussed in Section 4.

4 DISCUSSION: PROS AND CONS OF PROJECTION

In the preceding sections, we have discussed in some detail the problems that may occur with a numerical implementation of Taylor's algorithm and how adding a projection step greatly enhances the accuracy of remaining on the Taylor manifold. On a fundamental level, including a projection step in a numerical algorithm is commonplace: any discrete scheme that models an analytic system is, at its essence, simply a projection of the underlying continuous evolution. For many systems, small inaccuracies in the discretized system do not matter, and it is expected that increases in the resolution will bring the system ever closer to the true evolution. However in some cases, including that of the magnetostrophic system we have considered in this paper, certain quantities, namely the Taylor integral, must be maintained exactly (as zero). This is a troublesome constraint to deal with since it is non-linear, being quadratic in the magnetic field. Linear constraints on the other hand are much easier to deal with, a well-known example being incompressible fluid dynamics in which $\nabla \cdot \mathbf{u} = 0$ everywhere (the magnetic field obeys a similar constraint of $\nabla \cdot \mathbf{B} = 0$). Such a system may be evolved subject to this linear constraint by either simply using a representation in terms of a basis set that is divergence free (precisely the Galerkin method used in this paper), or by regarding the pressure as a Lagrange multiplier whose purpose is to impose the constraint. In this paper, to sidestep the issues attendant of non-linear constraints, we effectively linearize Taylor's condition about the magnetic field at each discrete time step, projecting its rate of change onto the tangent plane of the manifold. However, any linearization of a non-linear constraint will never be exact, and we discuss some of the pros and cons of the method below.

Let us begin by summarizing the positive points of the method. First, it is easy to implement once the Taylor tensor entries are computed, requiring only the assembly of a matrix and then computation of its singular value decomposition. Secondly, and perhaps more importantly, within any prescribed truncation of magnetic field, the method will *exactly* (up to numerical roundoff error) project the rate of change onto the tangent plane. It is worth noting that to capture the general magnetostrophic dynamics (and indeed, for the dynamics of a general system) we need to ensure that the system is converged in both time and space: that is, by ensuring that the evolution becomes independent of further increases in spatial resolution and further decreases in time step length. However with the projection method, at any fixed spatial truncation, the Taylorization depends only on the error incurred by time discretization and can be minimized by consideration of more accurate time-evolution methods. This should be compared to Taylor's original algorithm, in which the evolving Taylorization can be rendered zero only when the system is fully converged in both space *and* time. Therefore, as far as the Taylorization is concerned, the projection method allows us to ignore issues of spatial convergence with the knowledge that any non-zero Taylorization arises solely through errors in the temporal discretization.

The projection method, however, introduces some challenging technical issues. First is the construction of the Jacobian matrix J, describing the local tangent plane to the manifold, each entry being the contraction of the vector of magnetic field spectral coefficients with entries of the Taylor tensor. Not only might this become a computational bottleneck at large truncation, but we must take care that numerical inaccuracies do not creep in. The summation of floating point numbers is most accurate when they are all of similar magnitude. As we discussed in the text, using a Chebyshev representation mitigates this problem somewhat, but since the Taylor integral involves a spatial derivative, it will always be the case that smaller scales will be represented with larger Taylor tensor coefficients than those from the largest scales.

Second is a somewhat technical point, but the projection method requires us to distinguish between singular values of J which are zero, from those which are not. In a typical numerical output, there will be a subset of values which have a magnitude considerably larger than the remainder, but choosing a threshold criterion in advance (which must be valid for all such computations) may not be straightforward. However, it should be possible to sidestep this issue by noting that output from the singular value decomposition produces singular values ordered by their magnitude. Going down the list and deciding when the values drop off to zero is equivalent to projecting out the component associated with each singular vector in turn, and then checking that the vector produced is tangent to the manifold.

Third is the issue of truncation. Any numerical scheme is hostage to the resolution adopted; in our case, the issues are not only that the action of the differential operators are not fully resolved, but that the Taylor manifold itself may not be fully represented. That is, it may be that increasing the resolution may change the local curvature of the manifold, therefore altering the orientation of the local tangent plane and changing the subsequent evolution of the system. Of course, as in all numerical schemes, we anticipate that these discretization errors will decrease with increasing resolution and should be negligible if all the dynamics are properly resolved.

Finally, our linearized system will not be able to maintain accurately Taylor's constraint for all time. Eventually, due to temporal discretization error, or even numerical round-off error, the magnetic field will diverge from the manifold. If such an event were to occur,

then non-linear iterations could be performed to perturb the magnetic field to the closest place on the manifold (which always exists). How we find this location is not entirely straightforward; one possible method is to search in the direction normal to the tangent plane as discussed in Section 2.2. Having perturbed the system back onto the manifold the system can then be evolved as usual. If such a procedure was carried out when the deviation from the manifold was significant, it is possible that the required large perturbation may alter appreciably the flow and the subsequent dynamics (recall that the flow is dependent upon the magnetic field). With this in mind, it may be useful to consider a scheme which periodically perturbs the magnetic field, even if the deviation from the manifold is not large, to ensure that major adjustments are never required.

5 CONCLUSIONS

In an inertia-free inviscid geodynamo model, any magnetic field must evolve subject to a condition called Taylor's constraint. In this paper, we have discussed an algorithm that can be used to evolve a magnetic field subject to this constraint in a full-sphere. Central to the method is the spatial representation of the magnetic field in terms of an appropriate finite Galerkin global basis set. There then ensues not merely a projection but an exact reduction of the Taylor constraint onto a finite set of homogeneous quadratic conditions. This development allows an explicit construction of the tangent hyperplane at every point on the multidimensional Taylor manifold, and is the keystone to our algorithm. According to Taylor's method, the geostrophic flow arises to keep the evolution of the magnetic field on the manifold. However, as we have demonstrated, inaccuracies in computing u_g and in subsequent numerical projections mean that an evolution controlled in such a manner would quickly diverge from the manifold. As we have shown, incorporation of a projection step onto the local tangent plane keeps the solution trajectories on the manifold to high precision and is evidently stable.

It is noteworthy to add a comment on the choice of Galerkin basis. Our algorithm hinges on a finite characterization of Taylor's constraint which is only known for one class: polynomial radial basis functions combined with spherical harmonics. Thus our Galerkin scheme (satisfying both the boundary conditions and regularity at the origin) was built from these functions. A commonly considered variant for the Galerkin radial basis set is the spherical Bessel functions, the eigenfunctions of the free decay problem. However, no exact Taylor states can be found for any finite truncation (Livermore *et al.* 2008), essentially because Bessel functions do not combine in the same simple way as polynomials and the number of constraints exceeds the number of degrees of freedom. The required restriction of all possible Galerkin radial basis functions to those of polynomial type, may be viewed in a similar way to the use of spherical harmonics in solid angle. Alternative (θ, ϕ) representations exist, such as double Fourier series (Boyd 2001). However, in general, these will not have a polynomial representation in Cartesian coordinates and so will not combine, after transforming to a cylindrical geometry, in the manner required—as spherical Bessel functions do not in radius—to produce a small number of constraints. However, it is presumably the case that we can approximate a Taylor state using *any* spectral representation by using, for instance, a least-squares analysis. We would anticipate that, as the truncation increases, the error will converge to zero.

Finally, we comment briefly on the future directions of this work. The remaining piece required to evolve the magnetostrophic system is a method to find $\mathbf{u}_{\rm mag}$ as a function of a Taylor state $\mathbf{B}$ and temperature perturbation T. The method we envisage is adapting that used in Glatzmaier & Roberts (1995) for the absence of viscosity; developments in this direction are underway. In a spherical shell, compared to a full sphere, more complications arise. Not only must we consider a more potent Taylor's constraint [requiring more independent conditions satisfied compared with a full sphere (Livermore *et al.* 2010)], but in addition other constraints arise from considerations of continuity of the magnetostrophic component of flow across the tangent cylinder (Hollerbach & Proctor 1993). Although these additional conditions only apply at a single value of s, they apply to all wavenumbers of the Lorentz force (compared with only the axisymmetric component for Taylor's constraint) and may therefore locally strongly constrain the evolution of the magnetic field. The imposition of this augmented set of constraints may require subtle modifications to the algorithm as outlined earlier; this issue is currently under investigation.

ACKNOWLEDGMENTS

PWL was supported by NSF grant number 0724331 and NERC grant NE/G014043/1; AJ was supported by the European commission under contract number 028670. PWL would like to thank Emmanuel Dormy for useful discussions. The comments of two anonymous referees were helpful in improving the manuscript.

REFERENCES

Baumgarte, J., 1972. Stabilization of constraints and integrals of motion in dynamical systems, *Comp. Meth. Appl. Mech. Eng.,* **1,** 1–16.

Boyd, J.P., 2001. *Chebyshev and Fourier Spectral Methods,* Dover, New York.

Bullard, E.C. & Gellman, H., 1954. Homogeneous dynamos and terrestrial magnetism, *Phil. Trans. R. Soc. Lond. A,* **247,** 213–278.

Ciccotti, G., Ferrario, M. & Ryckaert, J.-P., 1982. Molecular dynamics of rigid systems in Cartesian coordinates: a general formulation, *Mol. Phys.,* **47**(6), 1253–1264.

Fearn, D., 1998. Hydromagnetic flow in planetary cores, *Rep. Prog. Phys.,* **61,** 175–235.

Fearn, D. & Proctor, M.R.E., 1987. On the computation of steady, self-consistent spherical dynamos, *Geophys. Astrophys. Fluid Dyn.,* **38,** 293–325.

Fox, B., Jennings, L.S. & Zomaya, A.Y., 2000. Constrained dynamics computations: models and case studies, in *Robotics and Intelligent Systems,* Vol. **16**, World Scientific, Singapore.

Frenkel, D. & Smit, B., 2002. *Understanding Molecular Simulation: From Algorithms to Applications,* 2nd edn, Elsevier, San Diego.

Gillet, N., Jault, D., Canet, E. & Fournier, A., 2010. Fast torsional waves and strong magnetic field within the Earth's core, *Nature,* **465**(74), 74–77.

Glatzmaier, G.A. & Roberts, P.H., 1995. A three-dimensional convective dynamo with rotating and finitely conducting inner core and mantle, *Phys. Earth planet. Inter.,* **91,** 63–75.

Hollerbach, R., 2000. A spectral solution of the magneto-convection equations in spherical geometry, *Int. J. Numer. Math. Fluids,* **32,** 773–797.

Hollerbach, R. & Ierley, G., 1991. A modal α^2-dynamo in the limit of asymptotically small viscosity, *Geophys. Astrophys. Fluid Dyn.,* **56,** 133–158.

Hollerbach, R. & Proctor, M.R.E., 1993. Non-axisymmetric shear layers in a rotating spherical shell, in *Solar and Planetary Dynamos,* pp. 145–152, eds Proctor et al., Cambridge University Press, Cambridge.

Hong, M., Choi, M.-H., Jung, S., Welch, S. & Trapp, J., 2005. Effective constrained dynamic simulation using implicit constraint enforcement, in *Proceedings of the 2005 IEEE International Conference on Robotics and Automation,* Barcelona, pp. 4520–4525.

Jault, D., Gire, C. & Le Mouel, J.L., 1988. Westward drift, core motions and exchanges of angular momentum between core and mantle, *Nature,* **333**(26), 353–356.

Kono, M. & Roberts, P.H., 2002. Recent geodynamo simulations and observations of the geomagnetic field, *Rev. Geophys.,* **40**(4), 1013, 1–53, doi:10.1029/2000RG00102.

Li, K., Livermore, P. & Jackson, A., 2010. An optimal Galerkin scheme to solve the kinematic dynamo eigenvalue problem in a full sphere, *J. Comp. Phys.,* **229**(23), 8666–8683.

Liu, J., Liu, X. & Ma, X., 2008. First-order perturbation of singular vectors in singular value decomposition, *IEEE Trans. Signal Process.,* **56**(7), 3044–3049.

Livermore, P., 2010. Galerkin orthogonal polynomials, *J. Comp. Phys.,* **229**(6), 2046–2060.

Livermore, P., Ierley, G. & Jackson, A., 2008. The structure of Taylor's constraint in three dimensions, *Proc. R. Soc. A,* **464,** 3149–3174.

Livermore, P., Ierley, G. & Jackson, A., 2009. The construction of exact Taylor states I: the full sphere, *Geophys. J. Int.,* **177**(2), 367–382.

Livermore, P., Ierley, G. & Jackson, A., 2010. The construction of exact Taylor states II: The influence of an inner core., *Phys. Earth planet. Inter.,* **178,** 16–26.

Marsden, J.E., Patrick, G.W. & Shkoller, S., 1998. Multisymplectic geometry, variational integrators, and nonlinear PDEs, *Comm. Math, Phys.,* **199,** 351–395.

Moffatt, H.K., 1969. The degree of knottedness of tangled vortex lines, *J. Fluid Mech.,* **35,** 117–129.

Müller, P., 1995. Ertel's potential vorticity theorem in physical oceanography, *Rev. Geophys.,* **33**(1), 67–95.

Press, W.H., Teukolsky, S.A., Vetterling, W.T. & Flannery, B.P., 1992. *Numerical Recipes in Fortran 77,* 2nd edn, Cambridge University Press Cambridge.

Rotvig, J. & Jones, C.A., 2002. Rotating convection-driven dynamos at low Ekman number, *Phys. Rev. E,* **66,** 056308:1–15.

Salmon, R., 2005. A general method for conserving quantities related to potential vorticity in numerical models, *Nonlinearity,* **18,** R1–R16.

Shampine, L.F., 1986. Conservation laws and the numerical solution of ODEs, *Comp. & Maths. with Appls.,* **12B,** 1287–1296.

Stellmach, S. & Hansen, U., 2004. Cartesian convection driven dynamos at low Ekman number, *Phys. Rev. E,* **70,** 056312,1–16.

Taylor, J.B., 1963. The magneto-hydrodynamics of a rotating fluid and the Earth's dynamo problem, *Proc. R. Soc. A,* **9,** 274–283.

Witkin, A., 1997. Physically based modeling: principles and practice—constrained dynamics, SIGGRAPH 1997 course notes.

APPENDIX A: ENUMERATION OF THE NON-ZERO ELEMENTS OF THE TAYLOR TENSOR

The Taylor integral (3) by be written in either of the following equivalent quadratic forms involving the spectral coefficients of magnetic field b_i:

$$\text{(i)}\ \ \mathcal{T}(s) \ = s^2\sqrt{1-s^2}\ \sum_{k=0}^{K}\sum_{i<j} T_{ijk}\, b_i\, b_j\, s^{2k},$$

$$\text{(ii)}\ \ \mathcal{T}(s) = s^2\sqrt{1-s^2}\ \sum_{k=0}^{K}\sum_{i<j} T_{ijk}\, b_i\, b_j\, \tilde{c}_k\, T_{2k}(s), \qquad \text{(A1)}$$

in what we denoted in the main text as the monomial or Chebyshev representation of the Taylor tensor. For the purposes of this Appendix, case (ii) may be viewed as a representation in terms of any general spanning set of polynomials, for instance, any family of orthogonal polynomials. The arguments that follow are in no way specific to Chebyshev polynomials. The range of k, bounded above by $K = L_{\max} + 2N_{\max} - 3$, takes into account the linear degeneracy caused by the electrically insulating external boundary conditions. The tensors T and $\tilde{T}$ are very sparse and it is of significant interest to enumerate the number of non-zero elements *NNZ*. In fact, we are only able to derive an upper bound (which in most cases is very tight) since we cannot rule out the possibility that some elements of the tensor are zero by chance.

Contributions to $\mathcal{T}(s)$ stem from consideration of every possible 'interaction' between two harmonics of indices i and j (where the index parametrizes dependence in both solid angle and radius) and is of the form

$$s^2\sqrt{1-s^2}\,Q_N(s^2),$$

where Q_N is a polynomial of known degree $N(i, j)$. Furthermore, to form a non-zero contribution, the two harmonics must obey certain selection rules as given in Livermore *et al.* (2008). We choose to write the Taylor tensors in a strictly upper triangular structure with $i < j$ to minimize the number of non-zero tensor entries. Table A1 summarizes the harmonic selection rules for the three distinct types of interaction (i) toroidal–poloidal (T–S), (ii) toroidal–toroidal (T–T) and (iii) poloidal–poloidal (S–S) between two harmonics of wavenumbers m_1 and m_2, degrees l_1 and l_2 and radial indices n_1 and n_2. Note that, aside from the structure as set out in (10) and satisfying the boundary conditions (11), the Galerkin radial basis functions are assumed arbitrary. That is, we assume only that they are of degree r^{l+1+2n} for given spherical harmonic l and radial index n but nothing whatsoever further (for instance, orthogonality is not assumed).

To enumerate the elements, there are two facts that must be borne in mind. First, as we set out above, if external electrically insulating boundary conditions are assumed then only the coefficients of $Q_N(\sigma)$ (denoting $\sigma = s^2$) up to degree $L_{\max} + 2N_{\max} - 3$ are independent. In addition, $Q_N(\sigma)$ contains a common factor of $\sigma^{\max(m-1,0)}$ (Livermore *et al.* 2008), which renders zero the first $\max(m-1, 0)$ coefficients in the monomial representation (i) but not necessarily in a more general representation (ii). In the former case, a typical interaction therefore supplies

$$\mathcal{A}(k) = \min\left[\frac{l_1+l_2-k}{2} + n_1 + n_2,\, L_{\max} + 2N_{\max} - 3\right] - \max(0, m-1) + 1$$

independent non-zero elements to T, where k takes the values 3, 2 and 4 for TS, TT and SS interactions, respectively. Note that we include all non-zero coefficients of Q_N (including s^0), hence the

Table A1. A summary of the selection rules, between (i) toroidal and poloidal harmonics, (ii) toroidal and toroidal harmonics and (iii) poloidal and poloidal harmonics of wavenumbers m_1 and m_2, degrees l_1 and l_2, and radial indices n_1 and n_2. If the rules are obeyed, then $Q_N(s^2)$ is non-zero and, other considerations notwithstanding (e.g. degeneracy due to boundary conditions), supplies $N + 1$ non-zero entries to the tensor T.

	TS	TT	SS
Selection	$m_1 = m_2$	$m_1 = m_2 \neq 0$	$m_1 = m_2 \neq 0$
rules	$l_1 - l_2 = 1 \pmod 2$	$l_1 - l_2 = 0 \pmod 2$	$l_1 - l_2 = 0 \pmod 2$
	same ϕ-phase	$l_1 \neq l_2$	if $l_1 = l_2$ then $n_1 \neq n_2$
		different ϕ-phase	different ϕ-phase
$2N$	$l_1 + l_2 - 3 + 2n_1 + 2n_2$	$l_1 + l_2 - 2 + 2n_1 + 2n_2$	$l_1 + l_2 - 4 + 2n_1 + 2n_2$

addition of the last term in the above expression. This may be contrasted with the more general representation (ii) (e.g. Chebyshev) in which a typical interaction supplies

$$\tilde{\mathcal{A}}(k) = \min\left[\frac{l_1 + l_2 - k}{2} + n_1 + n_2, L_{\max} + 2N_{\max} - 3\right] + 1,$$

independent non-zero elements to $\tilde{T}$. We shall now pursue the full enumeration for representation (i); that for representation (ii) is trivially obtained by interchanging $\mathcal{A}$ with $\tilde{\mathcal{A}}$ in the following. Note that, since $\mathcal{A}(k) \leq \tilde{\mathcal{A}}(k)$, of all possible representations of the Taylor tensor, that of the monomial representation has the smallest number of non-zero elements (as illustrated by Table 1).

In the TS case, the number of non-zero elements is of the form (suppressing the double sum over n_1 and n_2)

$$2\sum_{l_1\ \mathrm{odd}}\sum_{l_2\ \mathrm{even}}\mathcal{A}(3) + 2\sum_{l_1\ \mathrm{even}}\sum_{l_2\ \mathrm{odd}}\mathcal{A}(3) + \sum_{l_1\ \mathrm{even}}\sum_{l_2\ \mathrm{odd}}\mathcal{A}(3) + \sum_{l_1\ \mathrm{odd}}\sum_{l_2\ \mathrm{even}}\mathcal{A}(3).$$

In the above, the first two terms correspond to $m > 0$ and contain a factor of two for both cosine and sine terms in azimuth; the last two terms correspond to $m = 0$. By noting that $\mathcal{A}$ is symmetric in l_1 and l_2, the leftmost two summations are identical, as are the rightmost two.

The enumeration in the TT and SS cases follows similarly. However, since each of these involves harmonics of the same type (in contrast to those of the toroidal–poloidal interactions where the harmonics are of different type), by noting the restriction $i < j$ in (A1), we only need only consider azimuthal interactions where harmonic i has $\cos m\phi$ and harmonic j has $\sin m\phi$ dependence (and not vice versa).

The total enumeration of non-zero elements of the tensor T (in the monomial representation) is therefore

$$NNZ = \sum_{n_1=1}^{N_{\max}}\sum_{n_2=1}^{N_{\max}}\Bigg[\underbrace{2\sum_{\substack{eo\\ m=0}}\mathcal{A}(3) + \sum_{m>0}\left\{4\sum_{eo}\mathcal{A}(3)\right.}_{\mathrm{TS}} \underbrace{\sum_{oo+ee}\Phi_1}_{\mathrm{SS}} + \underbrace{\left.\sum_{oo+ee}\Phi_2\right\}}_{\mathrm{TT}}\Bigg], \tag{A2}$$

where

$$\Phi_1 = (1 - \delta_{l_1 l_2}\delta_{n_1 n_2})\mathcal{A}(4), \qquad \Phi_2 = (1 - \delta_{l_1 l_2})\mathcal{A}(2), \tag{A3}$$

and we have introduced the short-hand

$$\sum_{oo} = \sum_{l_1\ \mathrm{odd}}\sum_{l_2\ \mathrm{odd}}, \qquad \sum_{ee} = \sum_{l_1\ \mathrm{even}}\sum_{l_2\ \mathrm{even}}, \qquad \sum_{eo} = \sum_{l_1\ \mathrm{even}}\sum_{l_2\ \mathrm{odd}}. \tag{A4}$$

The summations over odd and even $l \geq m$ can be evaluated using

$$\sum_{l\ \mathrm{odd};\, l\geq m}^{L_{\max}} f(l) = \sum_{\lfloor m/2\rfloor}^{\lceil L_{\max}/2\rceil - 1} f(2i+1), \tag{A5}$$

$$\sum_{l\ \mathrm{even};\, l\geq m}^{L_{\max}} f(l) = \sum_{\max(0,\lceil m/2\rceil - 1)}^{\lfloor L_{\max}/2\rfloor - 1} f(2i+2), \tag{A6}$$

where $\lceil x\rceil$ and $\lfloor x\rfloor$ give the nearest integer greater than or less than x.

Due to the rather awkward structure of *NNZ*, we have been unable to simplify it into a closed form analytic expression; however, (A2) can be evaluated as it stands assisted by computer algebra. Note that, in either representations (i) or (ii), *NNZ* scales as $O(L_{\max}^6)$ (if $L_{\max} = N_{\max}$). This is due to the presence of five nested summations, each over the truncation, with the summand a linear function of $\mathcal{A}$, itself dependent on the spherical harmonic degree l and radial index n. Strictly speaking, *NNZ* is an upper bound for the number of non-zero elements since some coefficients of the relevant polynomials could be zero by chance. In fact, this does happen (although rarely and in an unpredictable manner). For example, in representation (i), it so happens that there is no coefficient of s^0 in

$$[{}_1\mathbf{S}_4, {}_1\mathbf{T}_9]$$

and the coefficient of the highest (expected) exponent of s^2 is also zero in the following interactions:

$$\left[{}_4\mathbf{S}_3^{3c}, {}_2\mathbf{T}_{10}^{3c}\right], \ \left[{}_2\mathbf{S}_{10}^{3c}, {}_4\mathbf{T}_3^{3c}\right], \ \left[{}_1\mathbf{S}_{12}^{7c}, {}_6\mathbf{T}_7^{7c}\right] \text{ and } \left[{}_6\mathbf{S}_7^{7c}, {}_1\mathbf{T}_{12}^{7c}\right].$$

Here, the notation $[{}_{n_1}\mathbf{S}_{l_1}^m, {}_{n_2}\mathbf{T}_{l_2}^m]$ (suppressing the azimuthal phase information) denotes the interaction between the poloidal mode of spherical harmonic degree and order, and radial degree (l_1, m_1, n_1) and the toroidal mode of indices (l_2, m_2, n_2). Adopting a Chebyshev representation, within the truncation $L_{\max} = 6$, $N_{\max} = 4$, no chance zeros occur, although four chance zeros do occur within the truncation $L_{\max} = 10$, $N_{\max} = 6$.

It is also briefly worth remarking that, within the truncated harmonics $0 \leq m \leq l \leq L_{\max}$ there exist magnetic fields for which not only are certain components of particular interactions zero (as noted earlier), but that have identically zero interaction with all harmonics. These are the rather special modes of toroidal type and of degree and order $L_{\max}$. Denoting such a toroidal field by $\mathbf{T}$ and any magnetic field (within the truncation) as $\mathbf{B}$, this means that $[\mathbf{T}, \mathbf{B}] = 0$, where the Taylor interaction $[\,,\,]$ is defined in (18). This result is entirely expected (and is therefore absent from the preceding discussion on 'chance' zeros) and follows directly from a combination of the harmonic selection rules given in Table A1 and the restriction of the truncation. Interestingly, it follows that $[\mathbf{T} + \epsilon\mathbf{B}, \mathbf{T} + \epsilon\mathbf{B}] = O(\epsilon^2)$ for arbitrary $\mathbf{B}$ and $\epsilon \ll 1$ and thus $\mathbf{T}$ has a Taylorization of zero which is 'stable' to linear perturbations.